Theory of the spin Seebeck effect in antiferromagnets

S. M. Rezende,[1,*] R. L. Rodríguez-Suárez,[1,2] and A. Azevedo[1]
[1]*Departamento de Física, Universidade Federal de Pernambuco, 50670-901, Recife, Pernambuco, Brazil*
[2]*Facultad de Física, Pontificia Universidad Católica de Chile, Casilla 306, Santiago, Chile*
(Received 20 October 2015; revised manuscript received 1 December 2015; published 19 January 2016)

The spin Seebeck effect (SSE) consists in the generation of a spin current by a temperature gradient applied in a magnetic film. The SSE is usually detected by an electric voltage generated in a metallic layer in contact with the magnetic film resulting from the conversion of the spin current into charge current by means of the inverse spin Hall effect. The SSE has been widely studied in bilayers made of the insulating ferrimagnet yttrium iron garnet (YIG) and metals with large spin-orbit coupling such as platinum. Recently the SSE has been observed in bilayers made of the antiferromagnet MnF_2 and Pt, revealing dependences of the SSE voltage on temperature and field very different from the ones observed in YIG/Pt. Here we present a theory for the SSE in structures with an antiferromagnetic insulator (AFI) in contact with a normal metal (NM) that relies on the bulk magnon spin current created by the temperature gradient across the thickness of the AFI/NM bilayer. The theory explains quite well the measured dependences of the SSE voltage on the sample temperature and on the applied magnetic field in MnF_2/Pt.

DOI: 10.1103/PhysRevB.93.014425

I. INTRODUCTION

The spin Seebeck effect (SSE), discovered in 2008 by Uchida and co-workers [1], refers to the generation of spin currents in magnetic materials by thermal gradients, and is the analog of the long-known thermoelectric Seebeck effect whereby a charge current is created by a temperature gradient in a metal [2–5]. The effect has been widely studied in structures containing metallic ferromagnets (FMs) such as permalloy, or insulating ferrimagnets such as yttrium iron garnet (YIG) [1–12]. The SSE is usually detected by the voltage created in a metallic layer (ML) attached to the FM layer as a result of the conversion of the spin current into a charge current by means of the inverse spin Hall effect (ISHE). The FM material can be a metal, a semiconductor, or an insulator, while the ML is made of a paramagnetic metallic material with strong spin-orbit coupling, such as Pt or Ta, or a FM material such as permalloy [13], or an antiferromagnetic metal such as IrMn [14,15]. Depending on the experimental arrangement, the spin current generated by the SSE can be perpendicular or parallel to the temperature gradient, characterizing the so-called transverse or longitudinal configurations, respectively. While the transverse SSE can be observed in both metallic and insulating magnetic materials, the longitudinal spin Seebeck effect (LSSE) is observed unambiguously only in insulators because they are free from the anomalous Nernst effect [16]. The longitudinal configuration has proved to be more interesting for scientific research and for applications such as in thermopower conversion devices [17]. There is currently intense effort to understand in detail the origins of the SSE and to find new materials and structures for possible applications.

Antiferromagnetic (AF) materials have been gaining renewed attention due to the emergence of AF spintronics [18–31]. Commonly employed passively to pin the magnetization of an adjacent ferromagnetic layer in spin-valve devices through the interfacial exchange bias [32–34], AF materials have very unique dynamic features that might have applications in novel devices [31]. They have been shown to be efficient spin current detectors by means of the spin Hall effect [14,15,25,28] and to be operative for dynamic spin pumping similarly to ferromagnets [26]. Two important recent developments have been the theoretical demonstration that the thermal coupling between antiferromagnetic insulators (AFIs) and normal metals (NMs) is relatively strong [29], and the experimental observation of the SSE in bilayers made of the antiferromagnet MnF_2 and Pt with SSE voltages comparable to those in ferromagnets [30]. Interestingly, the measured dependences of the SSE voltage in MnF_2/Pt on sample temperature and applied magnetic field are very different from the ones observed in YIG/Pt.

In this paper we present a theory for the SSE in AFI/NM structures that relies on the bulk magnon spin current created by the temperature gradient across the thickness of the bilayer. We show that in a two-sublattice antiferromagnet the spin currents carried by two magnon modes have opposite directions, so that a relatively intense magnetic field is necessary to produce a net magnon spin current. As in FMI/NM structures, part of the spin current in the AFI flows into the NM layer where it is converted to a charge current by the ISHE, producing a voltage proportional to the temperature gradient. The theory is applied to AFI/NM bilayers made with two well-known AF materials, MnF_2 and FeF_2. The calculated dependences of the SSE voltage on the sample temperature and on the applied field are in good qualitative agreement with the recent measurements of Wu *et al.* in MnF_2/Pt [30].

II. SPIN WAVES AND SPIN CURRENTS IN ANTIFERROMAGNETS

In this section we review the quantum approach to the properties of spin waves in a two-sublattice antiferromagnet and derive an expression for the spin current in terms of the two magnon modes of the spin excitations. We consider the Hamiltonian of an antiferromagnet consisting of contributions

*Corresponding author: rezende@df.ufpe.br

from Zeeman, exchange, and magnetic anisotropy energies in the form [35,36]

$$\mathrm{H} = -\gamma\hbar\sum_i \vec{S}_i \cdot \vec{H} + \sum_{i\neq j} 2J_{ij}\,\vec{S}_i\cdot\vec{S}_j - D\sum_i \left(S_i^z\right)^2, \quad (1)$$

where $\gamma = g\mu_B/\hbar$ is the gyromagnetic ratio, g is the spectroscopic splitting factor, μ_B is the Bohr magneton, $\hbar$ is the reduced Plank constant, $\vec{S}_i$ is the spin (in units of $\hbar$) at a generic lattice site i, $\vec{H}$ is the magnetic field considered to be uniform and lying in the z direction of a Cartesian coordinate system, J_{ij} is the exchange constant of the interaction between spins $\vec{S}_i$ and $\vec{S}_j$, and D is the uniaxial anisotropy constant. We treat the quantized excitations of the magnetic system with the approach of Holstein-Primakoff [37,38], which consists of transformations that express the spin operators in terms of boson operators that create or destroy magnons. In the first transformation the components of the local spin operators are related to the creation and annihilation operators of spin deviations at site i. Since there are two sublattices we introduce different spin deviation operators for each sublattice. Denoting the spins of the up and down sublattices by subscripts 1 and 2, respectively, we have in the linear approximation [35,36]

$$S_{1i}^{+} = (2S)^{1/2}\,a_i, \quad S_{1i}^{-} = (2S)^{1/2}\,a_i^{\dagger}, \quad S_{1i}^{z} = S - a_i^{\dagger}a_i, \quad (2)$$

$$S_{2i}^{+} = (2S)^{1/2}\,b_i^{\dagger}, \quad S_{2i}^{-} = (2S)^{1/2}\,b_i, \quad S_{2i}^{z} = -S + b_i^{\dagger}b_i, \quad (3)$$

where $a_i^{\dagger}$, a_i, and $b_i^{\dagger}$, b_i, are the creation and destruction operators for spin deviations at sites 1 and 2, which satisfy the boson commutation rules $[a_i,a_j^{\dagger}] = \delta_{ij}$, $[a_i,a_j] = 0$, $[b_i,b_j^{\dagger}] = \delta_{ij}$, and $[b_i,b_j] = 0$. The next step consists in introducing a transformation from the localized field operators to collective boson operators that satisfy the commutation rules $[a_k,a_{k'}^{\dagger}] = \delta_{kk}\ [a_k,a_{k'}] = 0$, $[b_k,b_{k'}^{\dagger}] = \delta_{kk'}\ [b_k,b_{k'}] = 0$,

$$a_i = N^{-1/2}\sum_k e^{i\vec{k}\cdot\vec{r}_i}\,a_k, \quad b_i = N^{-1/2}\sum_k e^{i\vec{k}\cdot\vec{r}_i}\,b_k, \quad (4)$$

where N is the number of spins in each sublattice and $\vec{k}$ is a wave vector. Using Eq. (4) in Eqs. (2) and (3) we obtain the Hamiltonian

$$\mathrm{H} = \sum_k \hbar\left(A_k a_k^{\dagger}a_k + B_k b_k^{\dagger}b_k + C_k a_k b_{-k} + C_k^{*}a_k^{\dagger}b_{-k}^{\dagger}\right), \quad (5)$$

where

$$A_k = \gamma(H_E + H_A + H), \quad B_k = \gamma(H_E + H_A - H), \quad (6)$$

$$C_k = \gamma\,H_E\,\gamma_k, \quad \gamma_k = (1/z)\sum_{\delta}\exp(i\,\vec{k}\cdot\vec{\delta}), \quad (7)$$

where we have assumed only nearest-neighbor intersublattice exchange interaction with parameter J, $H_E = 2SzJ/\gamma\hbar$ and $H_A = (2S-1)\,D/\gamma\hbar$ are, respectively, the effective exchange and anisotropy fields, z is the number, and $\vec{\delta}$ is the vector connecting nearest neighbors. In order to diagonalize the Hamiltonian in Eq. (5) we introduce a canonical transformation to new magnon operators obtained by linear combinations of the operators associated with the up and down sublattices [35,36],

$$a_k = u_k\alpha_k - v_k\beta_{-k}^{\dagger}, \quad (8)$$

$$b_{-k}^{\dagger} = -v_k\alpha_k + u_k\beta_{-k}^{\dagger}, \quad (9)$$

where $\alpha_k^{\dagger}$,α_k, and $\beta_k^{\dagger}$,β_k are the creation and destruction operators for the two magnon modes which satisfy the boson commutation rules. With the transformations (8) and (9) the Hamiltonian (5) becomes diagonal in the form

$$\mathrm{H} = \sum_k \hbar\left(\omega_{\alpha k}\alpha_k^{\dagger}\alpha_k + \omega_{\beta k}\beta_k^{\dagger}\beta_k\right), \quad (10)$$

where $\omega_{\alpha k}$ and $\omega_{\beta k}$ are the frequencies of the two magnon modes, given by

$$\omega_{\alpha k} = \omega_k + \gamma\,H, \quad \omega_{\beta k} = \omega_k - \gamma\,H, \quad (11)$$

$$\omega_k = \gamma\left[H_c^2 + H_E^2\left(1-\gamma_k^2\right)\right]^{1/2}, \quad (12a)$$

$$H_c = \left[H_A\left(2H_E + H_A\right)\right]^{1/2}, \quad (12b)$$

and the coefficients in Eqs. (8) and (9) that diagonalize the Hamiltonian are

$$u_k = \left(\frac{\omega_{ZB} + \omega_k}{2\omega_k}\right)^{1/2}, \quad v_k = \left(\frac{\omega_{ZB} - \omega_k}{2\omega_k}\right)^{1/2}, \quad (13)$$

where $\omega_{ZB} = \gamma(H_E + H_A)$ and $u_k^2 - v_k^2 = 1$. For a body-centered tetragonal lattice the structure factor in Eq. (7) becomes

$$\gamma_k = \cos(k_x a/2)\,\cos(k_y a/2)\,\cos(k_z c/2), \quad (14)$$

where a and c are the lattice parameters. The frequencies of the two magnon modes are minimum at the center of the Brillouin zone, $k = 0$, where $\gamma_k = 1$, $\omega_{\alpha 0} = \gamma\,(H_c + H)$, and $\omega_{\beta 0} = \gamma\,(H_c - H)$. As k increases both frequencies increase and reach the maximum values at the Brillouin zone boundary, where $\gamma_k = 0$, $\omega_\alpha = \omega_{ZB} + \gamma\,H$, and $\omega_\beta = \omega_{ZB} - \gamma\,H$. Note that, as the field increases, the frequency of the α mode increases while the one of the β mode decreases. If the field exceeds the critical value H_c the frequency $\omega_{\beta 0}$ becomes negative and there is a transition to the spin-flop phase, with the spin vectors pointing nearly in opposite directions and approximately perpendicular to the field.

The eigenstates of the Hamiltonian in Eq. (10) are denoted by $|n_{\alpha k}\rangle$ and $|n_{\beta k}\rangle$ and are generated by the successive application of the creation operators $\alpha_k^{\dagger}$ and $\beta_k^{\dagger}$ to the vaccum state $|0\rangle$. These states have a precisely defined number of magnons and uncertain phase, and they have vanishing transverse components of the spin, as can be seen by the relations $\langle n_{\alpha k}|\alpha_k\,|n_{\alpha k}\rangle = 0$ and $\langle n_{\beta k}|\beta_k\,|n_{\beta k}\rangle = 0$. In order to establish a correspondence between classical and quantum spin waves one should use the concept of coherent magnon states [39], defined in analogy to the coherent photon states introduced by Glauber [40]. In an antiferromagnet the coherent states corresponding to the two magnon modes are defined as the eigenstates of the annihilation operators,

$$\alpha_k\,|c_k\rangle = c_k\,|c_k\rangle, \quad \beta_k\,|d_k\rangle = d_k\,|d_k\rangle, \quad (15)$$

where the eigenvalues c_k and d_k are complex numbers. Although the coherent states are not eigenstates of the

Hamiltonian and as such do not have a well-defined number of magnons, they have nonzero expectation values for the spins S_1^+ and S_2^+ with a well defined phase. It can be shown that the numbers of magnons in the coherent states $|c_k\rangle$ and $|d_k\rangle$ are, respectively, $|c_k|^2$ and $|d_k|^2$. Using Eqs. (2)–(9) and (15) one can obtain the expectation values of the spins in the two sublattices in the coherent magnon state $|c_k\rangle$,

$$\begin{aligned} \langle c_k|S_1^+|c_k\rangle &= (2S/N)^{1/2} u_k c_k e^{-i\omega_{\alpha k}t}, \\ \langle c_k|S_1^z|c_k\rangle &= S - (1/N)\, u_k^2\, |c_k|^2, \end{aligned} \tag{16}$$

$$\begin{aligned} \langle c_k|S_2^+|c_k\rangle &= -(2S/N)^{1/2} v_k c_k e^{-i\omega_{\alpha k}t}, \\ \langle c_k|S_2^z|c_k\rangle &= -S + (1/N)\, v_k^2\, |c_k|^2, \end{aligned} \tag{17}$$

where, for simplicity, we have omitted the exponential spatial dependence. This result is consistent with the semiclassical picture [26,41], whereby in the α_k mode both up and down spins undergo a circular clockwise precession with frequency $\omega_{\alpha k}$ and tilted with angles that are proportional to the square root of the magnon number and with ratio u_k/v_k. Similarly, for the β_k mode the spins are in counterclockwise precession with frequency $\omega_{\beta k}$ and with angles with the ratio v_k/u_k.

Finally, we derive an expression for the spin current carried by magnons in the antiferromagnet with simple arguments. The total z component of the spin angular momentum carried by magnons is given by $S^z = \sum_i (S_{1i}^z + S_{2i}^z)$. With Eqs. (2)–(4) and (15) one can show that the operator that has nonzero expectation value in magnon states is given by

$$S^z = \sum_k \hbar[-\alpha_k^\dagger \alpha_k + \beta_k^\dagger \beta_k]. \tag{18}$$

The opposite signs in the angular momenta of the two modes is consistent with the semiclassical picture of the spins precessing in opposite directions. Since the two magnon modes have the same group velocity $\vec{v}_{mk} = \hat{k}\, \partial\omega_k/\partial k$, the spin current density operator is

$$\vec{J}_S^z = \frac{\hbar}{V} \sum_k \vec{v}_{mk}[-\alpha_k^\dagger \alpha_k + \beta_k^\dagger \beta_k]. \tag{19}$$

In the Appendix we present a more formal derivation of this equation. Note that the spin current in an antiferromagnet vanishes when the magnon numbers in the two modes are the same, as previously pointed out in Ref. [42].

III. THEORY FOR THE SPIN SEEBECK EFFECT IN ANTIFERROMAGNETS

The bulk magnon spin current model has been developed for the LSSE in ferromagnets and successfully applied to explain quantitatively a variety of experimental data in YIG/Pt [43,44]. Here we extend the model to a bilayer structure made of an antiferromagnetic insulator, such as MnF_2 and FeF_2, and a normal metal with strong spin-orbit coupling, such as Pt. The AFI/NM is subject to a temperature gradient across the thickness of the bilayer, as illustrated in Fig. 1. While in the FMI/NM bilayer the spin current created by the thermal gradient is carried by one magnon mode, here the spin current has contributions from the two magnon modes. A fraction

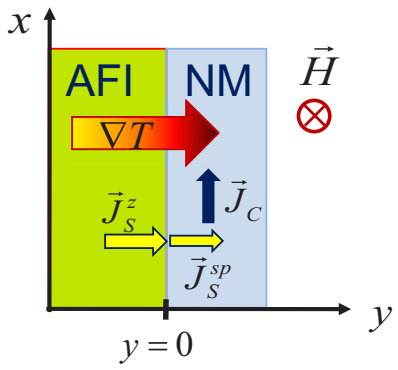

FIG. 1. Illustration of the antiferromagnetic insulator (AFI)/normal metal (NM) bilayer structure employed to investigate the spin Seebeck effect showing the coordinate axes, the magnon spin current produced by the temperature gradient, and the charge current generated by the ISHE in the NM.

of the spin current in the AFI flows into the NM layer and is converted into a transverse charge current by the ISHE [45–47] producing the dc voltage at the ends. The magnon spin current due to the thermal gradient across the thickness can be calculated with the Boltzmann equation imposing the appropriate boundary conditions. We choose a coordinate system with the z axis parallel to the magnetic field H applied in the plane along the easy axis of the AFI, and the y axis perpendicular to the plane, as shown in Fig. 1. Denote by $n_{\mu k}$ the number of magnons in the $\mu = \alpha, \beta$ mode with wave number k in the whole volume V of the AFI layer, by $n_{\mu k}^0$ the number in thermal equilibrium, given by the Bose-Einstein distribution,

$$n_{\mu k}^0 = \frac{1}{e^{\hbar\omega_{\mu k}/k_B T} - 1}, \tag{20}$$

and by $\delta n_{\mu k}(\vec{r}) = n_{\mu k}(\vec{r}) - n_{\mu k}^0$ the number in excess of equilibrium. Since the contributions of the two modes to the spin current have opposite signs, we define the magnon accumulation $\delta n_m(\vec{r})$ as

$$\delta n_m(\vec{r}) = \frac{1}{(2\pi)^3} \int d^3k \left[\left(n_{\alpha k} - n_{\alpha k}^0\right) - \left(n_{\beta k} - n_{\beta k}^0\right)\right], \tag{21}$$

and the bulk magnon spin current density with polarization z is [43,44,48,49]

$$\vec{J}_S^z = \frac{\hbar}{(2\pi)^3} \int d^3k\, \vec{v}_{mk} \left[\left(n_{\alpha k}(\vec{r}) - n_{\alpha k}^0\right) - \left(n_{\beta k}(\vec{r}) - n_{\beta k}^0\right)\right], \tag{22}$$

where $\vec{v}_{mk}$ is the k magnon velocity. The distribution of the magnon number under the influence of a thermal gradient can be calculated with the Boltzmann transport equation [50]. In the absence of external forces and in the relaxation approximation, in steady state the Boltzmann equation gives for each magnon mode

$$n_{\mu k}(\vec{r}) - n_{\mu k}^0 = -\tau_{\mu k} \vec{v}_{mk} \cdot \vec{\nabla} n_{\mu k}^0 - \tau_{\mu k} \vec{v}_{mk} \cdot \vec{\nabla}\left[n_{\mu k}(\vec{r}) - n_{\mu k}^0\right], \tag{23}$$

where $\tau_{\mu k}$ is the μk magnon relaxation time. Using Eq. (23) in Eq. (22) one can show that the spin current is the sum of two

parts, $\vec{J}_S^z = \vec{J}^z_{S\vec{\nabla}T} + \vec{J}^z_{S\delta n}$, where

$$\vec{J}^z_{S\vec{\nabla}T} = -\frac{\hbar}{(2\pi)^3}\int d^3k\left[\tau_{\alpha k}\frac{\partial n^0_{\alpha k}}{\partial T} - \tau_{\beta k}\frac{\partial n^0_{\beta k}}{\partial T}\right]\vec{v}_{mk}(\vec{v}_{mk}\cdot\vec{\nabla}T) \tag{24}$$

is the contribution of the flow (convection) of magnons due to the temperature gradient and

$$\vec{J}^z_{S\delta n} = -\frac{\hbar}{(2\pi)^3}\int d^3k[\tau_{\alpha k}\vec{v}_{mk}\vec{v}_{mk}\cdot\vec{\nabla}\delta n_{\alpha k} - \tau_{\beta k}\vec{v}_{mk}\vec{v}_{mk}\cdot\vec{\nabla}\delta n_{\beta k}] \tag{25}$$

is due to the spatial variation of the magnon accumulation. With the temperature gradient normal to the plane, Eq. (24) gives the spin current in the y direction

$$J_S^z = S_S^z\vec{\nabla}T, \tag{26}$$

$$S_S^z = \frac{\hbar^2}{6\pi^2 k_B T^2}\int dk\, k^2 v_{mk}^2\left[\frac{e^{\hbar\omega_{\beta k}/k_BT}\,\omega_{\beta k}}{\eta_{\beta k}(e^{\hbar\omega_{\beta k}/k_BT}-1)^2} - \frac{e^{\hbar\omega_{\alpha k}/k_BT}\,\omega_{\alpha k}}{\eta_{\alpha k}(e^{\hbar\omega_{\alpha k}/k_BT}-1)^2}\right], \tag{27}$$

where T is the average temperature and $\eta_{\mu k} = 1/\tau_{\mu k}$ is the μk magnon relaxation rate. We consider the magnon and phonon systems to have the same temperature T [51]. Equation (27) contains the most relevant dependences of the SSE on the sample temperature and applied field. It shows, for instance, that the spin current, and hence the SSE, vanishes for $H = 0$, at any temperature, because the two modes have the same occupancy, as previously predicted theoretically [42] and confirmed by experiments [30]. In order to calculate the full expression for the spin current in the NM layer it is necessary to consider the contribution from the magnon diffusion given by Eq. (25), the spin pumping process resulting from the magnon accumulation at the AFI/NM interface, and the boundary conditions at the surface and interfaces, as it has been done for FMI/NM bilayers [43,44]. Here we aim at describing the dependences of the SSE in AFI/NM structures on temperature and field, so we simply consider that the spin current in the NM layer is proportional to the term in Eq. (26),

$$J_S^z(0) = C\, g_{\rm eff}^{\uparrow\downarrow}\, S_S^z\,\vec{\nabla}T, \tag{28}$$

where C is a factor that involves the thickness of the AFI layer, the magnon diffusion length, and other material parameters [43,44], and $g_{\rm eff}^{\uparrow\downarrow}$ is the real part of the effective spin mixing conductance at the interface that takes into account the spin-pumped and backflow spin currents [52]. Due to the inverse spin Hall effect, the spin current density $\vec{J}_S^z$ flowing into the NM generates a charge current density given by $\vec{J}_C = \theta_{SH}(2e/\hbar)\,\vec{J}_S^z \times \vec{\sigma}$, where θ_{SH} is the spin-Hall angle and $\vec{\sigma}$ is the spin polarization [45–47], and produces a SSE voltage at the ends of the NM layer. Since the spin current at the AFI/NM interface diffuses into the NM [52] with diffusion length λ_N, in order to calculate the voltage at the ends of the NM layer one has to integrate the charge current density along x and y so that the SSE voltage becomes [46,47,53]

$$V = R_N w\lambda_N\frac{2e}{\hbar}\theta_{SH}\tanh\left(\frac{t_N}{2\lambda_N}\right)J_S^z(0), \tag{29}$$

where R_N, t_N, and w are, respectively, the resistance, thickness, and width of the NM layer. Thus, with Eqs. (28) and (29) we have for the spin Seebeck effect voltage

$$V_{\rm SSE} = R_N\, w\lambda_N\frac{2e}{\hbar}\theta_{SH}\tanh\left(\frac{t_N}{2\lambda_N}\right)C\, g_{\rm eff}^{\uparrow\downarrow}\, S_S^z\,\vec{\nabla}T. \tag{30}$$

As in FMI/NM bilayers, the SSE voltage is proportional to the temperature gradient across the magnetic layer, to the spin mixing conductance of the interface, and to the spin-Hall angle of the NM. The dependences of the voltage on the sample temperature and on the applied field are contained mainly in the spin Seebeck coefficient S_S^z.

IV. SPIN SEEBECK EFFECT IN MnF_2 AND FeF_2

In this section we apply the SSE theory for two antiferromagnetic insulators that attracted considerable attention in the past, namely, the fluorides FeF_2 and MnF_2. Both crystallize in the tetragonal rutile structure exhibiting simple three-dimensional (3D) antiferromagnetic ordering with two sublattices at temperatures below the Néel temperature T_N and have had their magnetic, thermodynamic, and dynamic properties extensively studied [54]. Their magnetic interactions are dominated by nearest-neighbor exchange, having effective intersublattice exchange fields on the same order of magnitude, $H_E \approx 550$ kOe, and consequently similar Néel temperatures, $T_N \approx 67$ and 78 K, respectively, for MnF_2 and FeF_2 [54]. In FeF_2 the ground state configuration of its magnetic Fe^{2+} ions is $3d^5(^5D_4)$, which has a finite orbital angular momentum and consequently a large effective anisotropy field $H_A = 190$ kOe, arising from the single-ion spin-orbit coupling [55,56]. The large uniaxial anisotropy of FeF_2 makes it a prototype 3D Ising system with its characteristic critical behavior at the AF-paramagnetic transition at T_N [57,58]. On the other hand, in MnF_2 the ground state configuration of the magnetic Mn^{2+} ions is $3d^5(^6S_{5/2})$, with no orbital angular momentum and thus very small single-ion anisotropy. The origin of the magnetic anisotropy of MnF_2 lies mainly in the dipolar interaction, which is sizable in the tetragonal arrangement of the magnetic ions $H_A \approx 8$ kOe [59,60], but much smaller than in FeF_2. The representation of the magnetic anisotropy of MnF_2 in the form of Eq. (1) is an approximation that holds very well for most applications.

For the numerical evaluation of the integral in Eq. (27) we assume a spherical Brillouin zone with radius $k_m \sim \pi/a$ and use an approximate expression for the structure factor in Eq. (14), $\gamma_k = \cos(\pi\, k/2k_m)$, so that the magnon dispersion relation in Eq. (12) becomes $\omega_k = \gamma\,[\,H_c^2 + H_E^2\sin^2(\pi\, k/2k_m)]^{1/2}$. Figure 2(a) shows the frequency versus wave number measured in MnF_2 by inelastic neutron scattering at $T = 3$ K in zero field [61]. The frequency increases from 0.27 THz at the zone center to 1.63 THz at the zone boundary due to the effect of exchange. The thick curve in Fig. 2(a) is the fit of Eq. (12) to data obtained with $g = 2.0$, $H = 0$, $H_A = 8.02$ kOe, and $H_E = 575$ kOe, demonstrating

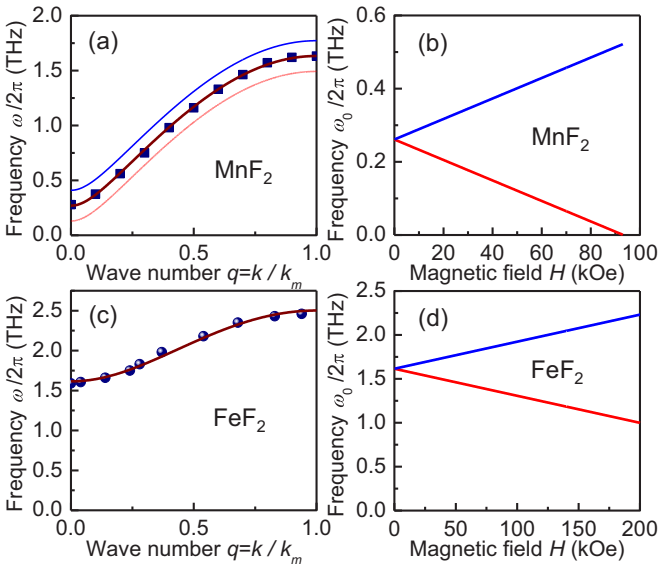

FIG. 2. Magnon frequencies in MnF_2 and FeF_2 at low temperatures. In (a) and (c) the symbols represent inelastic neutron scattering data of Refs. [61,63] at $H = 0$ and the solid curves are the dispersion relations calculated with Eqs. (11) and (12). In (a) the two thin curves correspond to $H = 50$ kOe. (b) and (d) show the variation of the $k = 0$ frequencies with magnetic field intensity.

that it represents quite well the actual dispersion. This value of H_E is larger than the actual intersublattice exchange field because Eq. (12) does not take into account the intrasublattice exchange that exists in MnF_2. The thin curves are the dispersion relations for the two magnon modes with $H = 50$ kOe. In Fig. 2(b) we show the behavior with field of the zone-center magnon frequencies. The frequency of the down mode (β) goes to zero at $H = H_c$ where there is the transition from the AF to the spin-flop (SF) phase. The stability limit of the AF phase has been accurately measured in MnF_2 by antiferromagnetic resonance (AFMR) techniques [62]. The value $H_c = 92.9$ kOe measured at $T = 4.2$ K is a little smaller than the one calculated with Eq. (12b) and the fields obtained from the fit because the intrasublattice exchange does not contribute to the zone-center frequency.

FeF_2 has much larger anisotropy than MnF_2 so that the magnon frequencies over the whole Brillouin zone lie in the few terahertz range, as shown in Fig. 2(c). The inelastic neutron scattering data of Ref. [63], shown in the figure, can be fitted with Eq. (12) with $g = 2.2$, $H = 0$, $H_A = 192$ kOe and $H_E = 620$ kOe. As in MnF_2, the value of H_E is larger than the actual intersublattice exchange field because of the effect of the intrasublattice exchange. In FeF_2 the $k = 0$ magnon (AFMR) frequency in zero field is 1.6 THz and its properties have been studied in detail with far-infrared lasers [64]. The field dependence of the AFMR frequency in Fig. 2(d) shows that even with a field as high as $H = 200$ kOe the frequency of the down mode is 1 THz. The spin-flop transition ($H_{SF} \approx$ 500 kOe) has been investigated only with very high pulsed magnetic fields [65] existing in few facilities in the world. Note that, as recently shown [66], the high magnon frequencies in AFIs might also be used to operate spin-transfer-torque nano-oscillators with terahertz frequency driven by dc electric currents.

In order to evaluate the integral in Eq. (27) one needs the magnon group velocity $v_{mk} = \partial\omega_k/\partial k$, which is the same for both modes. From Eq. (12) with the approximate structure factor for the tetragonal lattice one obtains

$$v_{mk} = \frac{\gamma^2 H_E^2 \pi}{4 k_m} \frac{\sin(\pi q)}{\omega_k}, \tag{31}$$

where $q = k/k_m$ is the normalized wave number. With this expression the coefficient in Eq. (27) becomes

$$S_S^z = \frac{k_m \gamma^4 H_E^4 \hbar^3}{24 k_B^2} B_s, \tag{32a}$$

$$B_s = \frac{1}{T^3} \int dq\, q^2 \frac{1}{x^2} \sin^2(\pi q) \times \left[\frac{e^{x_\beta} x_\beta}{\eta_{\beta k} (e^{x_\beta} - 1)^2} - \frac{e^{x_\alpha} x_\alpha}{\eta_{\alpha k} (e^{x_\alpha} - 1)^2} \right], \tag{32b}$$

where $x = \hbar\omega_k/k_B T$ and $x_\mu = \hbar\omega_{\mu k}/k_B T$ are normalized energies.

Initially we apply the theory for the SSE to MnF_2, for which there are recent experimental results by Wu *et al.* [30]. The integral in Eq. (32b) can be evaluated numerically using the magnon dispersion in Eqs. (11) and (12) with $g = 2.0$, $H_A = 8.02$ kOe, and $H_E = 575$ kOe, and magnon relaxation rates with dependences on q, T, and H. These dependences, which have decisive roles in determining the behavior of the SSE with varying temperature and field, can be obtained with a combination of experimental and theoretical inputs. The magnon damping in MnF_2, measured with high-resolution inelastic neutron scattering at $T = 30$ K in zero field [67], can be represented very well by $\eta_k = (0.06 + 7.5\, q^2 - 6.0\, q^3) \times 10^{11}\ \mathrm{s}^{-1}$. We have calculated the magnon relaxation rate due to four-magnon processes, as in Refs. [35,36], and used the data to determine the adjustable parameters in the theory. The result agrees quite well with the q-dependent terms of the measured damping, so we use the four-magnon relaxation calculation to obtain the temperature and field dependences of $\eta_{\mu k}$ for the two modes. The calculated T dependence for q in the range 0.10–0.40, from where most contribution to the integral in Eq. (32) comes, is $\eta_k \approx aT^3$, which is also in agreement with experiments [67]. Thus we use $\eta_{\mu k}(q, H, T) = \eta_0 + a_{H\mu}(7.5\, q^2 - 6.0\, q^3)\,(T/30)^3 \times 10^{11}\ \mathrm{s}^{-1}$, where η_0 is the residual damping, considered an adjustable parameter, and $a_{H\mu}$ is a factor that expresses the field dependence for each mode. This has been calculated numerically for $q = 0.2$ and fixed T and fitted with the following expressions:

$$T = 5\,\mathrm{K}: a_{H\alpha} = 1 + 0.04H + 0.014\,(e^{0.09H} - 1), \quad a_{H\beta} = 1 + 0.0005H + 0.095\,(e^{0.047H} - 1), \tag{33}$$

$$T = 10\,\mathrm{K}: a_{H\alpha} = 1 + 0.01H + 0.008\,(e^{0.068H} - 1), \quad a_{H\beta} = 1 + 0.0005H + 0.074(e^{0.034H} - 1), \tag{34}$$

and for $T > 20$ K, $a_{H\alpha} \approx a_{H\beta} \approx 1$, where H is in kOe.

Figure 3(a) shows the calculated dependence of the SSE voltage in MnF_2/Pt on the magnetic field intensity for four

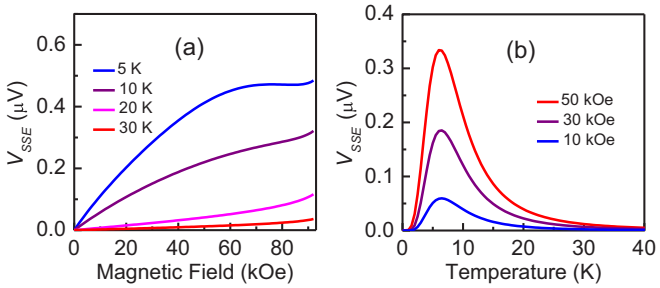

FIG. 3. Dependences of the SSE voltage in MnF_2/Pt on the magnetic field H (a) and on the temperature (b), calculated with Eq. (29).

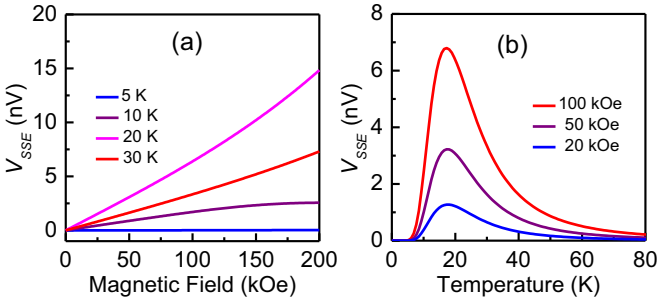

FIG. 4. Dependences of the SSE voltage in FeF_2/Pt on the magnetic field H (a) and on the temperature (b), calculated with Eq. (29).

temperature values. We have used in the calculation $\eta_0 = 1.2 \times 10^8\ \mathrm{s}^{-1}$ for the residual damping, which is the value that best reproduces the initial slope of the experimental data at $T = 5\,\mathrm{K}$. The other adjustable parameter is the factor relating the voltage with the integral in the spin-Seebeck coefficient, $V_{\mathrm{SSE}} = FB_S$. We used $F = 1.5 \times 10^{15}\ \mu\mathrm{VK}^3\,\mathrm{s}^{-1}$ so as to obtain a value for the plateau similar to the experimental data at $T = 5\,\mathrm{K}$ [30]. At any temperature the voltage vanishes for zero field, because the two modes have the same thermal occupation and the same relaxation rate, so their spin currents cancel out. The voltage increases continuously with field up to close to the spin-flop transition where the slope changes abruptly. Note that at low T, as the field increases the thermal number of the down-going (β) mode increases while the number of the up-going (α) mode decreases. At the same time, the relaxation rate of the α mode increases faster than that in the β mode, so that the difference between the two terms in Eq. (32b) increases faster. This explains why the initial slope is larger at lower temperatures. In Fig. 3(b) we show the variation of the SSE voltage with temperature for several field values, calculated with the same expression for the relaxation rate and voltage factor but with $a_{H\alpha} = a_{H\beta} = 1$. The qualitative agreement of the curves in Figs. 3(a) and 3(b) with the experimental data of Wu *et al.* [30] is quite good. Of course, the quantitative comparison of theory with experiments would require the full treatment of the problem including magnon diffusion and spin pumping.

One might be surprised that the SSE voltages measured in MnF_2/Pt at $T = 5\,\mathrm{K}$ are comparable to those in YIG/Pt at $T = 300\,\mathrm{K}$, since MnF_2 besides being an antiferromagnet has a magnon energy gap two orders of magnitude larger than that in YIG and thus relatively smaller thermal number. The reason for this is twofold and is based on the fact that in the bulk magnon SSE model the spin current is determined by the thermal numbers and the relaxation rate. First, the density of states of gap magnons with $q \approx 0$ is negligible, and in YIG at $T = 300\,\mathrm{K}$ the magnons that contribute most to the SSE have $q \approx 0.3$–0.5. Since the frequency of the zone-boundary magnons in YIG is on the order of 7 THz, the modes with $q \approx 0.3$–0.5 have frequency in the range 1–3 THz, which is larger than in MnF_2. The second reason is that in MnF_2 at $T = 5\,\mathrm{K}$ the magnon relaxation rate in the important wave number range is $\eta_k \approx 2 \times 10^8\ \mathrm{s}^{-1}$, while in YIG at $T = 300\,\mathrm{K}$ it is two orders of magnitude larger [43].

The calculation of the SSE for FeF_2/Pt was done following the same route used for MnF_2/Pt. The integral in Eq. (32b) was evaluated numerically using the magnon dispersion in Eqs. (11) and (12) with $g = 2.2$, $H_A = 192\,\mathrm{kOe}$, $H_E = 620$ kOe, and the magnon relaxation rates. These were calculated numerically with four-magnon scattering processes, as in Refs. [35,36], and fitted with $\eta_{\mu k} = \eta_0 + 7.5\, a_{H\mu}\, q^3\, (T/20)^3 \times 10^{10}\ \mathrm{s}^{-1}$, where η_0 is the residual damping, and $a_{H\mu}$ is a factor that expresses the field dependence for each mode. The factors were calculated numerically for fixed T and $q = 0.4$, where the integrand in Eq. (32b) peaks, and fitted with the following expressions:

$$T = 5\,\mathrm{K} : a_{H\alpha} = 1 + 0.477\,(e^{0.03H} - 1),$$
$$a_{H\beta} = 1 + 0.505\,(e^{0.032H} - 1), \tag{35}$$

$$T = 10\,\mathrm{K} : a_{H\alpha} \approx a_{H\beta} = 1 + 0.23\,(e^{0.0195H} - 1),$$
$$T > 20\,\mathrm{K} : .\ a_{H\alpha} \approx a_{H\beta} \approx 1, \tag{36}$$

where the field H is in kOe. We use for the residual damping the value $\eta_0 = 2 \times 10^9\ \mathrm{s}^{-1}$ obtained from the extrapolation to $T = 0$ of the data in Ref. [55] and for the voltage factor the same value used for MnF_2/Pt, $F = 1.5 \times 10^{15}\ \mu\mathrm{VK}^3\,\mathrm{s}^{-1}$, to allow a comparison. Figures 4(a) and 4(b) show the results for the SSE voltage dependences, respectively on the magnetic field intensity for four temperature values and on the temperature for several values of H. Figure 4(b) shows the voltage only up to 200 kOe because this is the maximum field that is available in most laboratories. The first obvious difference from MnF_2/Pt is that the voltage is two orders of magnitude smaller. This is due to three facts: (1) The higher magnon frequencies in FeF_2 that result in smaller thermal magnon numbers compared to MnF_2; (2) the smaller group velocity in FeF_2, as clearly seen in Fig. 2(c); and (3) the larger magnon relaxation. For the same reasons, the dependence of the voltage on H in Fig. 4(a) is quite different from the one in Fig. 3(a), especially at low T. The voltage is negligible at $T = 5\,\mathrm{K}$, increases with increasing T, and only for $T > 20\,\mathrm{K}$ does it decrease as in MnF_2/Pt. However, the dependence of the voltage on T with fixed field shown in Fig. 4(b) is similar to that for MnF_2/Pt in Fig. 3(b). Although the SSE voltage in FeF_2/Pt is in the nanovolt range, it might be experimentally

detected, as in recent observations of the SSE in paramagnets [68].

In summary, we have presented a model for the spin Seebeck effect in bilayers made of an antiferromagnetic insulator and a normal metal, based on the bulk magnon spin current created by the temperature gradient across the thickness of the AFI/NM. As in FMI/NM structures, the spin current generated in the AFI flows into the NM layer where it is converted to a charge current by the inverse spin-Hall effect, producing a voltage proportional to the temperature gradient. The theory is applied to AFI/NM bilayers made with two well-known AF materials, MnF_2 and FeF_2. The calculated dependences of the SSE voltage on the sample temperature and on the applied field are in good qualitative agreement with the recent measurements of Wu *et al.* in MnF_2/Pt [30].

ACKNOWLEDGMENT

This research was supported in Brazil by Conselho Nacional de Desenvolvimento Científico e Tecnológico (CNPq), Coordenação de Aperfeiçoamento de Pessoal de Nível Superior (CAPES), Financiadora de Estudos e Projetos (FINEP), and Fundação de Amparo à Ciência e Tecnologia do Estado de Pernambuco (FACEPE) and in Chile by Fondo Nacional de Desarrollo Científico y Tecnológico (FONDECYT) No. 1130705.

APPENDIX: DERIVATION OF THE SPIN CURRENT DENSITY IN AN AFI

Consider the exchange interaction between the spins $\vec{S}_{1i}$ and $\vec{S}_{2j}$ of the two sublattices 1 and 2 described by the second term in Eq. (1),

$$E_{1i} = 2J \sum_j \vec{S}_{1i} \cdot \vec{S}_{2j}, \tag{A1}$$

where we have considered only the intersublattice exchange interaction. To find the expression for the exchange spin current in the antiferromagnet we apply the continuum approximation to $\vec{S}_{1i}$ and $\vec{S}_{2j}$. In Eq. (A1) we write $\vec{S}_{1i}$ as $\vec{S}_1(\vec{r})$ and its neighboring spin $\vec{S}_{2j}$ as $\vec{S}_2(\vec{r}+\vec{a})$, where $\vec{r}$ represents a position vector and $\vec{a}$ is the displacement vector of the j site in sublattice 2, relative to the i site in sublattice 1. $\vec{S}_{2j} = \vec{S}_2(\vec{r}+\vec{a})$ is expanded as

$$\vec{S}_2(\vec{r}+\vec{a}) = \vec{S}_2(\vec{r}) + \frac{\partial \vec{S}_2}{\partial \vec{r}} \cdot \vec{a} + \frac{1}{2}\frac{\partial^2 \vec{S}_2}{\partial \vec{r}^2} a^2. \tag{A2}$$

Due to symmetry the second term in the expansion vanishes in the sum in Eq. (A1) so that the the dominant term in the expansion is the third one and higher-order terms are neglected. Thus, the exchange effective field is

$$\vec{H}_{\rm exch} = -\frac{1}{\gamma\,\hbar}\frac{\delta E_{1i}(\vec{S})}{\delta \vec{S}_{1i}} = -\frac{2Ja^2 z}{\gamma\,\hbar}\frac{\partial^2 \vec{S}_2}{\partial \vec{r}^2} = -\frac{A}{M_2}\nabla^2 \vec{M}_2, \tag{A3}$$

where z is the number of nearest neighbors, $\vec{M}_{1,2}$ represents the sublattice magnetizations, and $A = 2Ja^2 zS/\gamma\,\hbar$ is the stiffness parameter. Using this exchange field in the Landau-Lifshitz equation of motion for $\vec{M}_1$ we obtain

$$\frac{\partial \vec{M}_1}{\partial t} = -\gamma \frac{A}{M_2}\vec{M}_1 \times \nabla^2 \vec{M}_2 = -\vec{\nabla} \cdot \left(\gamma \frac{A}{M_2}\vec{M}_1 \times \nabla_v \vec{M}_2\right). \tag{A4}$$

Equation (A4) has the form of the conservation of angular momentum $\partial \vec{M}/\partial t = -\vec{\nabla} \cdot \vec{J}_{Mv}$, so that one can write for the magnetization current density in the y direction [48,69]

$$\vec{J}_{My} = \gamma \frac{A}{M_2}\left(\vec{M}_1 \times \frac{\partial}{\partial y}\vec{M}_2\right). \tag{A5}$$

From this equation, we can show that the z-polarized spin current density in the y direction, related to the magnetization current by $J_S^z = J_M^z/\gamma$, is given by

$$J_S^z = -i\,\frac{A}{2M_2}\left[-m_1^+ \frac{dm_2^-}{dy} + m_1^- \frac{dm_2^+}{dy}\right], \tag{A6}$$

where $m_i^{\pm} = m_{ix} \pm i m_{iy}$. Using the linear transformations given by Eqs. (2) and (3), we can write the circular components of the magnetization in terms of the local creation and annihilation operators of spin deviations,

$$m_1^+ = \left(\frac{\gamma\hbar}{V}\right)\sqrt{2S}\sum_i a_i, \quad m_1^- = \left(\frac{\gamma\hbar}{V}\right)\sqrt{2S}\sum_i a_i^\dagger, \tag{A7}$$

$$m_2^+ = \left(\frac{\gamma\hbar}{V}\right)\sqrt{2S}\sum_i b_i^\dagger, \quad m_2^- = \left(\frac{\gamma\hbar}{V}\right)\sqrt{2S}\sum_i b_i, \tag{A8}$$

Using the transformations given by Eqs. (4) we can express the spin current (A6) in terms of the collective boson operators a_k and b_k,

$$J_S^z = \frac{\gamma\,\hbar A}{V}\left[\sum_k k\,(a_k b_{-k} + a_k^\dagger b_{-k}^\dagger)\right]. \tag{A9}$$

Finally, with the transformations (8) and (9) to the magnon operators we have in the normal order

$$J_S^z = -\frac{\gamma\,\hbar A}{V}\sum_k 2u_k v_k k(\alpha_k^\dagger \alpha_k - \beta_k^\dagger \beta_k), \tag{A10}$$

where the coefficients u_k and v_k are given by Eq. (13) and we have disregarded products of operators for different modes because they give vanishing expectation values for any magnon state. From Eqs. (11)–(13) we can show that $2u_k v_k = \gamma H_E \gamma_k/\omega_k$. Considering the simple geometrical factor $\gamma_k = \cos ka$ and $ka \ll 1$, consistent with the continuum approximation, the group velocity obtained from Eq. (12) is

$$v_{mk} = \frac{\partial \omega_k}{\partial k} = \frac{2\gamma^2 H_E^2 \gamma_k a^2 k}{2\omega_k} = \gamma\, H_E a^2 k(2u_k v_k), \tag{A11}$$

so that with $H_E = 2SzJ/\gamma\,\hbar$ the spin current density in terms of the two magnon mode operators becomes

$$J_S^z = -\frac{\hbar}{V}\sum_k v_{mk}(\alpha_k^\dagger \alpha_k - \beta_k^\dagger \beta_k), \tag{A12}$$

which is the same as Eq. (19) obtained with heuristic arguments.

[1] K. Uchida, S. Takahashi, K. Harii, J. Ieda, W. Koshibae, K. Ando, S. Maekawa, and E. Saitoh, Nature (London) **455**, 778 (2008).

[2] G. E. W. Bauer, E. Saitoh, and B. J. van Wees, Nat. Mater. **11**, 391 (2012).

[3] H. Adachi, K. Uchida, E. Saitoh, and S. Maekawa, Rep. Prog. Phys. **76**, 036501 (2013).

[4] S. R. Boona, R. C. Myers, and J. P. Heremans, Energy Environ. Sci. **7**, 885 (2014).

[5] K. Uchida, M. Ishida, T. Kikkawa, A. Kirihara, T. Murakami, and E. Saitoh, J. Phys.: Condens. Matter **26**, 343202 (2014).

[6] K. Uchida, J. Xiao, H. Adachi, J. Ohe, S. Takahashi, J. Ieda, T. Ota, Y. Kajiwara, H. Umezawa, H. Kawai, G. E. W. Bauer, S. Maekawa, and E. Saitoh, Nat. Mat. **9**, 894 (2010).

[7] K. Uchida, T. Ota, K. Harii, K. Ando, H. Nakayama, and E. Saitoh, Solid State Commun. **150**, 524 (2010).

[8] K. Uchida, H. Adachi, T. Ota, H. Nakayama, S. Maekawa, and E. Saitoh, Appl. Phys. Lett. **97**, 172505 (2010).

[9] K. Uchida, T. Nonaka, T. Ota, H. Nakayama, and E. Saitoh, Appl. Phys. Lett. **97**, 262504 (2010).

[10] C. M. Jaworski, J. Yang, S. Mack, D. D. Awschalom, J. P. Heremans, and R. C. Myers, Nat. Mater. **9**, 898 (2010).

[11] A. Slachter, F. L. Bakker, J. P. Adam, and B. J. van Wees, Nat. Phys. **6**, 879 (2010).

[12] Y. Onose, T. Ideue, H. Katsura, Y. Shiomi, N. Nagaosa, and Y. Tokura, Science **329**, 297 (2010).

[13] B. F. Miao, S. Y. Huang, D. Qu, and C. L. Chien, Phys. Rev. Lett. **111**, 066602 (2013).

[14] J. B. S. Mendes, R. O. Cunha, O. Alves Santos, P. R. T. Ribeiro, F. L. A. Machado, R. L. Rodriguez-Suarez, A. Azevedo, and S. M. Rezende, Phys. Rev. B **89**, 140406 (R) (2014).

[15] W. Zhang, M. B. Jungfleisch, W. Jiang, J. E. Pearson, A. Hoffmann, F. Freimuth, and Y. Mokrousov, Phys. Rev. Lett. **113**, 196602 (2014).

[16] T. Kikkawa, K. Uchida, Y. Shiomi, Z. Qiu, D. Hou, D. Tian, H. Nakayama, X.-F. Jin, and E. Saitoh, Phys. Rev. Lett. **110**, 067207 (2013).

[17] A. B. Cahaya, O. A. Tretiakov, and G. E. W. Bauer, IEEE Trans. Magn. **51**, 0800414 (2015).

[18] A. S. Núñez, R. A. Duine, P. Haney, and A. H. MacDonald, Phys. Rev. B **73**, 214426 (2006).

[19] A. B. Shick, S. Khmelevskyi, O. N. Mryasov, J. Wunderlich, and T. Jungwirth, Phys. Rev. B **81**, 212409 (2010).

[20] A. H. MacDonald and M. Tsoi, Philos. Trans. R. Soc., A **369**, 3098 (2011).

[21] V. M. T. S. Barthem, C. V. Colin, H. Mayaffre, M.-H. Julien, and D. Givord, Nat. Commun. **4**, 2892 (2013).

[22] P. Merodio, A. Ghosh, C. Lemonias, E. Gautier, U. Ebels, M. Chshiev, H. Béa, V. Baltz, and W. E. Bailey, Appl. Phys. Lett. **104**, 032406 (2014).

[23] C. Hahn, G. de Loubens,V. V. Naletov, J. BenYoussef, O. Klein, and M. Viret, Europhys. Lett. **108**, 57005 (2014).

[24] E. V. Gomonay and V. M. Loktev, Low Temp. Phys. **40**, 17 (2014).

[25] H. Chen, Q. Niu, and A. H. MacDonald, Phys. Rev. Lett. **112**, 017205 (2014).

[26] R. Cheng, J. Xiao, Q. Niu, and A. Brataas, Phys. Rev. Lett. **113**, 057601 (2014).

[27] J. Zelezny, H. Gao, K. Vyborny, J. Zemen, J. Masek, A. Manchon, J. Wunderlich, J. Sinova, and T. Jungwirth, Phys. Rev. Lett. **113**, 157201 (2014).

[28] W. Zhang, M. B. Jungfleisch, F. Freimuth, W. Jiang, J. Sklenar, J. E. Pearson, J. B. Ketterson, Y. Mokrousov, and A. Hoffmann, Phys. Rev. B **92**, 144405 (2015).

[29] A. Brataas, H. Skarsvåg, E. G. Tveten, and E. L. Fjaerbu, Phys. Rev. B **92**, 180414(R) (2015).

[30] S. M. Wu, W. Zhang, Amit K. C., P. Borisov, J. E. Pearson, J. S. Jiang, D. Lederman, A. Hoffmann, and A. Bhattacharya, arXiv:1509.00439.

[31] T. Jungwirth, X. Marti, P. Wadley, and J. Wunderlich, arXiv:1509.05296.

[32] S. S. P. Parkin *et al.*, J. Appl. Phys. **85**, 5828 (1999).

[33] J. Nogués and I. K. Schuller, J. Magn. Magn. Mater. **192**, 203 (1999).

[34] J. R. Fermin, M. A. Lucena, A. Azevedo, F. M. de Aguiar, and S. M. Rezende, J. Appl. Phys. **87**, 6421 (2000).

[35] S. M. Rezende and R. M. White, Phys. Rev. B **14**, 2939 (1976).

[36] S. M. Rezende and R. M. White, Phys. Rev. B **18**, 2346 (1978).

[37] M. Sparks, *Ferromagnetic Relaxation* (Mc Graw-Hill, New York, 1964).

[38] R. M. White, *Quantum Theory of Magnetism*, 3rd ed. (Springer-Verlag, Berlin, 2007).

[39] S. M. Rezende and N. Zagury, Phys. Lett. **29A**, 47 (1969); N. Zagury and S. M. Rezende, Phys. Rev. B **4**, 201 (1971).

[40] R. J. Glauber, Phys. Rev. **131**, 2766 (1963).

[41] F. Kefferand C. Kittel, Phys. Rev. **85**, 329 (1952).

[42] S. M. Rezende, R. L. Rodríguez-Suárez, J. C. López Ortiz, and A. Azevedo, Phys. Rev. B **87**, 014423 (2013).

[43] S. M. Rezende, R. L. Rodríguez-Suárez, R. O. Cunha, A. R. Rodrigues, F. L. A. Machado, G. A. Fonseca Guerra, J. C. López Ortiz, and A. Azevedo, Phys. Rev. B **89**, 014416 (2014).

[44] S. M. Rezende, R. L. Rodríguez-Suárez, R. O. Cunha, J. C. López Ortiz, and A. Azevedo, J. Magn. Magn. Mater. **400**, 171 (2016).

[45] E. Saitoh, M. Ueda, H. Miyajima, and G. Tatara, Appl. Phys. Lett. **88**, 182509 (2006).

[46] A. Hoffmann, IEEE Trans. Magn. **49**, 5172 (2013).

[47] J. Sinova, S. O. Valenzuela, J. Wunderlich, C. H. Back, and T. Jungwirth, Rev. Mod. Phys. **87**, 1213 (2015).

[48] Y. Kajiwara, K. Harii, S. Takahashi, J. Ohe, K. Uchida, M. Mizuguchi, H. Umezawa, K. Kawai, K. Ando, K. Takanashi, S. Maekawa, and E. Saitoh, Nature (London) **464**, 262 (2010).

[49] S. S.-L. Zhang and S. Zhang, Phys. Rev. Lett. **109**, 096603 (2012).

[50] F. Reif, *Fundamentals of Statistical and Thermal Physics* (Mc Graw-Hill, New York, 2008).

[51] M. Agrawal,V. I. Vasyuchka, A. A. Serga, A. D. Karenowska, G. A. Melkov, and B. Hillebrands, Phys. Rev. Lett. **111**, 107204 (2013).

[52] Y. Tserkovnyak, A. Brataas, and G. E. W. Bauer, Phys. Rev. B **66**, 224403 (2002); Y. Tserkovnyak, A. Brataas, G. E. W. Bauer, and B. I. Halperin, Rev. Mod. Phys. **77**, 1375 (2005).

[53] A. Azevedo, L. H. Vilela-Leão, R. L. Rodríguez-Suárez, A. F. Lacerda Santos, and S. M. Rezende, Phys. Rev. B **83**, 144402 (2011).

[54] L. J. de Jongh and A. R. Miedema, Adv. Phys. **50**, 947 (2001).

[55] R. C. Ohlmann and M. Tinkham, Phys. Rev. **123**, 425 (1961).
[56] M. T. Hutchings, B. D. Rainford, and H. J. Guggenheim, J. Phys. C: Solid State Phys. **3**, 307 (1970).
[57] M. Chirwa, L. Lundgren, P. Nordblad, and O. Beckman, J. Magn. Magn. Mater. **15-18**, 457 (1980).
[58] D. P. Belanger, P. Nordblad, A.R. King, V. Jaccarino, L. Lundgren, and O. Beckman, J. Magn. Magn. Mater. **31-34**, 1095 (1983).
[59] F. Keffer, Phys. Rev. **87**, 608 (1952).
[60] J. Barak, V. Jaccarino, and S. M. Rezende, J. Magn. Magn. Mater. **9**, 323 (1978).
[61] S. P. Bayrakci, T. Keller, K. Habicht, and B. Keimer, Science **312**, 1926 (2006).
[62] S. M. Rezende, A. R. King, R. M. White, and J. P. Timbie, Phys. Rev. B **16**, 1126 (1977).
[63] B. D. Rainford, J. G. Houmann, and H. J. Guggenheim, in *Proceedings of the Symposium on Inelastic Scattering of Neutrons in Solids and Liquids* (IAEA, Vienna, 1972), p. 655.
[64] R. W. Sanders, V. Jaccarino, and S. M. Rezende, Solid State Commun. **28**, 907 (1978).
[65] V. Jaccarino, A. R. King, M. Motokawa, T. Sakakibara, and M. Date, J. Magn. Magn. Mater. **31**, 1117 (1983).
[66] R. Cheng, D. Xiao, and A. Brataas, arXiv:1509.09229.
[67] S. P. Bayrakci, D. A. Tennant, Ph. Leininger, T. Keller, M. C. R. Gibson, S. D. Wilson, R. J. Birgeneau, and B. Keimer, Phys. Rev. Lett. **111**, 017204 (2013).
[68] S. M. Wu, J. E. Pearson, and A. Bhattacharya, Phys. Rev. Lett. **114**, 186602 (2015).
[69] C. Heide, Phys. Rev. Lett. **87**, 197201 (2001).